PRELIMINARY RESULTS OF AN EXPERIMENTAL AND COMPUTATIONAL ANALYSIS ON THE BEHAVIOR OF WEB-FLANGE JUNCTIONS OF GFRP PULTRUDED PROFILES SUBJECTED TO CONCENTRATED LOADS

L. Feo[1*], A.S. Mosallam[2], R. Penna[1]

[1]*Department of Civil Engineering, University of Salerno, 84084, Fisciano (SA), Italy*
[2]*Department of Civil & Env. Engineering, University of California, Irvine, 92697, CA, USA*
**l.feo@unisa.it*

Keywords: Pultruded Composites, Web-Flange Junction, Mechanical Testing, FEA

Abstract
This paper presents a summary of preliminary results obtained from an experimental and numerical investigation on the behavior of web-flange junctions of pultruded glass fibre-reinforced polymer I-profiles. The pull-out strengths derived from fifteen tests are presented and typical modes failure are identified. Finite element results support experimental findings from strain gage data.

1 Introduction

Fibre-reinforced polymer (FRP) composites represent a class of advanced materials whose use has spread from the aeronautical, mechanical and naval industry to civil infrastructure due to their high strength-to-weight ratio, low maintenance cost and high corrosion resistance.
The majority of the commercially-produced pultruded fibre-reinforced polymers (PFRP) have been designed and developed by the pultrusion industry and are intended for low-stress applications.
Recently, composites have been introduced as primary structural members to replace or complement other conventional materials, such as steel, concrete and wood, in critical applications such as bridge decks, pedestrian bridges, and recently in highway bridges and other infrastructural systems.
As the interest in using PFRP profiles in construction applications continues to increase, it became critical and essential to understand their short- and long-term mechanical behavior. Several recent and relevant studies [1-9] have been conducted and focused on the performance of PFRP frame structures. The results of these studies have highlighted the major problems associated with the structural deficiency of unidirectional PFRP profiles, especially at the web-flange junctions (WFJ) that lack fibre continuity. This lack of fibre continuity may lead to progressive degradation in both axial and rotational stiffnesses and strength of these junctions, affecting both the buckling, post-buckling and the overall short- and long-term structural integrity of the PFRP profiles [1-7].
Other relevant studies [8,9] have highlighted the influence of the architecture of the web-flange junctions on the collapse of the profiles. In fact, the mechanical properties of the WFJ are not the same as those of the flats parts of the web and the flanges due to them also

depending on the specific processing method used by the manufacturer to produce PFRP profiles.
The authors are developing a research program whose main aim is to evaluate the strength and stiffness characteristics of open-web PFRP profiles. In particular, both the axial and rotational stiffness of WFJ of I- profiles and C- profiles are investigated through in-depth experimental program in order to develop P-δ and M-θ relations that are necessary for accurate analytical predictions of both the local and global responses of PFRP frame structures. In fact, their failure mechanism has yet to be fully understood and they often involve failure of the web-flange junctions. Moreover, P-δ and M-θ relations are also essential for establishing optimum and reliable design limit-states of such structures.
In particular, this paper presents preliminary results obtained from the first series of pull-out experimental tests on GFRP pultruded I-profiles. The experimental findings are compared with the numerical results obtained through a finite element analysis (FEA) carried out using commercial FEA software.

2 Experimental Setup

2.1 Test description

The test program was conducted in the Materials and Structural Testing Laboratory of the Department of Civil Engineering (DICIV) of the University of Salerno. It consisted of two main parts: the first part was an evaluation of the axial behavior for web-flange junctions of the profiles, while the second part was an evaluation of web-flange relative rotational behavior.
This paper describes the results of the first part of the research giving details of the pullout full-scale experiments of the aforementioned FRP profiles.
In the pullout tests, WFJ from different profiles are subjected to a uniform pull load applied on the bottom flange of the profiles. Specifically, two different test setup were considered: in the first, the pull force was eccentrically applied at the end-point of the specimens (Fig. 1) while, in the second, the pull force was applied at their mid-point (Fig. 2). These loading scenarios are similar to those reported in Ref. [1].

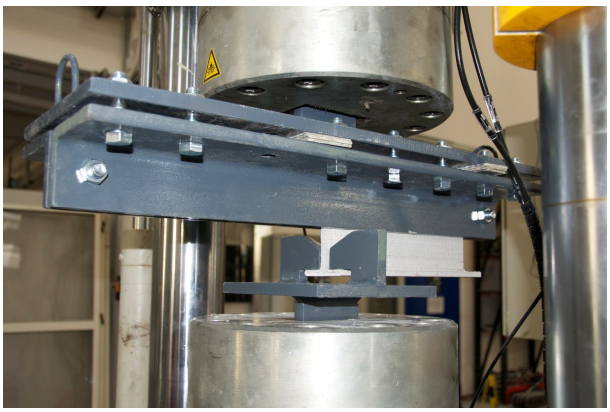

Figure 1. End Point Pull-Out Test Setup.

Figure 2. Mid Point Pull-Out Test Setup.

For all the specimens, the pull axial load was performed using a calibrated *Shenck Hydropuls* servo-hydraulic testing machine equipped with two thick steel angles in order to provide fixity to the upper flange and web of the profiles (Fig. 3). In order to measure the web/flange junction strains of the specimens, three rectangular self temperature compensated strain gages (*Vishay MM C2A-06-125LW-120*) were placed as shown in Figs. 4a,b. In all the tests, a force-controlled loading protocol was adopted and both the incremental applied load as well as the associated relative web/flange displacement were continuously recorded via a calibrated data

acquisition system (*System 5100 Vishay MM*). Data obtained during the test were subsequently elaborated using the *StrainSmart* software.

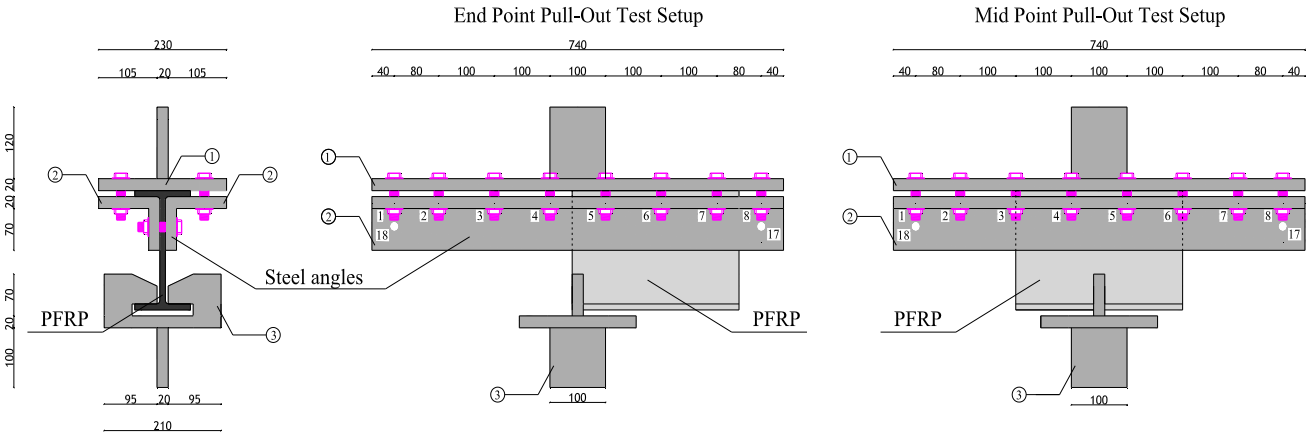

Figure 3. Schematic Setup of Web-Flange Junction Pull-Out Test (*dimension in mm*).

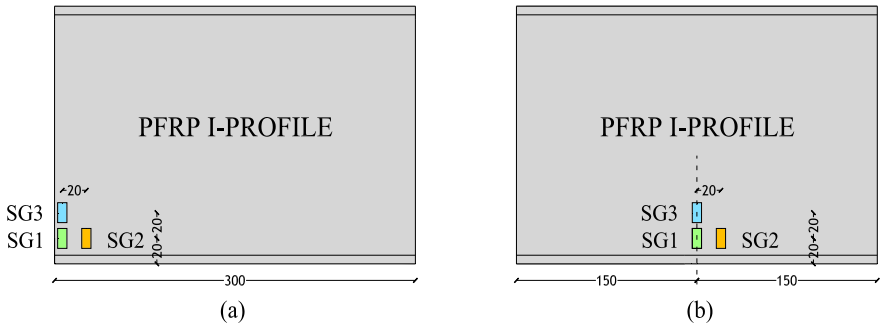

Figures 4a,b. Typical strain gages layout for End Point Pull-Out (a) and Mid Point Pull-Out Test (b) (*dimension in mm).*

2.2 PFRP materials

Two sizes of commercially-produced structural pultruded I- profiles, i.e., 160 (H) x 80 (B) x 8 (T_f=T_w) mm and 200 (*H*) x 100 (*B*) x 10 mm (T_f=T_w), denoted as *I_160* and *I_200*, respectively, were chosen for this investigation. The geometrical characteristics of the PFRP profiles discussed in this paper are reported in Table 1.

Profile	**H [mm]**	**B [mm]**	**T_f [mm]**	**T_w [mm]**	**A x 10^3 [mm^2]**	**g [g/m]**	**I_{xx} x 10^6 [mm^4]**
I_160	160	80	8	8	2.49	4.480	9.66
I_200	200	100	10	10	3.89	6.990	23.60

Table 1. Geometry of the pultruded profiles.

The mechanical properties of the FRP materials obviously depend on the matrix and fibre volume ratios, which, for pultruded GFRP elements, are generally equal to 60% and 40%, respectively, assuming no presence of voids.

As it is well-known [10,11], the pultruded FRP shapes can be simulated as a laminated configuration with the internal layer constituted of unidirectional fibres (*roving*) parallel to the longitudinal axis (*z*) and the external layers composed of multi-directional fibres (*mat*) which completely wind around the pultruded element. Consequently, the material exhibits a transversely isotropic behavior: anisotropic in the *z*-direction and isotropic in the *x* and *y*

directions. In the aforementioned coordinate system (*x*, *y* and *z*) the engineering constants are related as follow: $E_x = E_y$; $\nu_{zx} = \nu_{zy}$ and $G_{zx} = G_{zy}$.
The nominal values of the main mechanical properties of the pultruded profiles were supplied by the manufactures (Table 2) and verified by the authors through traction tests.

Property	**Measurement Unit**	**Value**
Longitudinal elastic modulus, E_z	MPa	23,000
Transversal elastic moduli, $E_x = E_y$	MPa	8,500
Transversal shear modulus, G_{xy}	MPa	3,455
Shear Moduli, $G_{zx} = G_{zy}$	MPa	3,000
Longitudinal Poisson's ratio, ν_{xy}		0.23
Transversal Poisson's ratios, $\nu_{zx} = \nu_{zy}$		0.09
Material density (γ)	kg/m^3	1,600-1,800

Table 2. Mechanical properties of GFRP structural profiles (Nominal values).

3 Experimental Results

A total of 15 specimens were cut transversely from the I-profiles and loaded in tension at a constant rate of about 0.001 N/s until failure. In particular, they were divided into four group according to the profile size (*I_160* and *I_200*) and location of the pull force (*End-Point* and *Mid-Point*). The detailed results obtained from the experimental investigation are presented in Tables 3-6.
Typical load versus displacement curves, obtained from tests on *I_200_MP* and *I_200_EP* specimens, are shown in Fig. 5 and Fig. 6, respectively.
As shown in Fig. 5, the *I_200_MP_1* specimen displacement increased linearly with increasing load up to an axial displacement of 0.9 mm, corresponding to a load level of 14.8 kN. After which, a stiffness degradation was observed and the load-displacement (P-δ) curve followed a near-linear behavior until a 1.18 mm displacement level was reached (corresponding to a 17.9 kN axial load). Beyond this level, signs of local junction failure started to occur. This failure increases rapidly and determines a large region of separation between the flange and web as shown in Fig. 7a. For the *I_200_EP_1* specimen, the displacement increased linearly with an increasing load up to an axial displacement of 0.46 mm, corresponding to a load level of 6.29 kN. After which, failure started to occur. This failure increases rapidly and determines a large region of separation between the flange and web as shown in Fig. 8a.
For the *I_200_EP_2* specimen the displacement increased linearly with increasing load up to an axial displacement of 0.6363 mm, corresponding to a load level of 5.0063 kN. After this load level failure occurs as shown in Fig. 9a.
The deformations along the y-axis (ε_{yy}) recorded during the test of specimens *I_200_MP_1* *I_200_EP_1* and *I_200_EP_2* are plotted in Figs.7b, 8b and 9b, respectively.

4 Finite Element Analysis

In order to support the experimental findings, a 3-D finite element analysis was employed in the linear elastic field by using commercial finite-element software (*Straus 7* by G+D Computing). In particular, the internal parts of the web and flanges of the pultruded profiles, composed of unidirectional fibres (*roving*), were modeled by using eight-node orthotropic finite elements (*bricks*), while orthotropic surface elements (*plates*) were used to simulate the external layers composed of multi-directional fibres (*mat*). The mechanical properties of the materials used for the analysis are reported in Table 2.
Figures 10.a and 10.b show the three-dimensional finite-element meshes of specimens *I_200_EP_1 (I_200_EP_2)* and *I_200_MP_1*, respectively. In both cases, the nodes of the

plates of the upper flange were constrained against all movements, while the uniform pull load acting on the lower flange of the PFRP I-profile was applied by modeling the steel device fixed to the testing machine.

Specimens	**Length [mm]**	**Failure Load [kN]**	**$\delta_{failure}$ [mm]**
I_160_EP_1	300	3.7942	1.1049
I_160_EP_2	300	3.1160	0.6484
I_160_EP_3	300	4.1862	1.1598
I_160_EP_4	300	3.2489	0.5367

Table 3. Failure loads and displacements obtained from experimental tests on *I_160_EP* specimens.

Specimens	**Length [mm]**	**Failure Load [kN]**	**$\delta_{failure}$ [mm]**
I_160_MP_1	300	10.3826	0.5776
I_160_MP_2	300	9.2705	1.0952
I_160_MP_2	300	9.3582	1.0095
I_160_MP_4	300	11.2126	1.5285

Table 4. Failure loads and displacements obtained from experimental tests on *I_160_MP* specimens.

Specimens	**Length [mm]**	**Failure Load [kN]**	**$\delta_{failure}$ [mm]**
I_200_EP_1	300	6.2900	0.4600
I_200_EP_2	300	5.0063	0.6363
I_200_EP_3	300	8.0428	0.9373
I_200_EP_4	300	5.2407	0.7011

Table 5. Failure loads and displacements obtained from experimental tests on *I_200_EP* specimens.

Specimens	**Length [mm]**	**Failure Load [kN]**	**$\delta_{failure}$ [mm]**
I_200_MP_1	300	17.9000	1.1800
I_200_MP_2	300	13.7920	1.4838
I_200_MP_3	300	15.0095	1.5137

Table 6. Failure loads and displacements obtained from experimental tests on *I_200_MP* specimens.

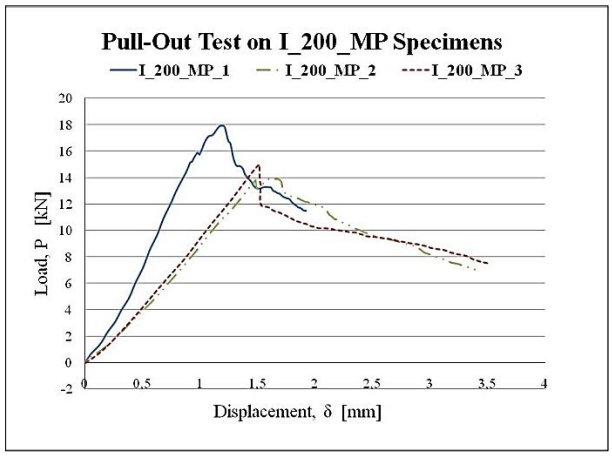

Figure 5. Load (P) versus displacement (δ) curve for *I_200_MP* group of specimens.

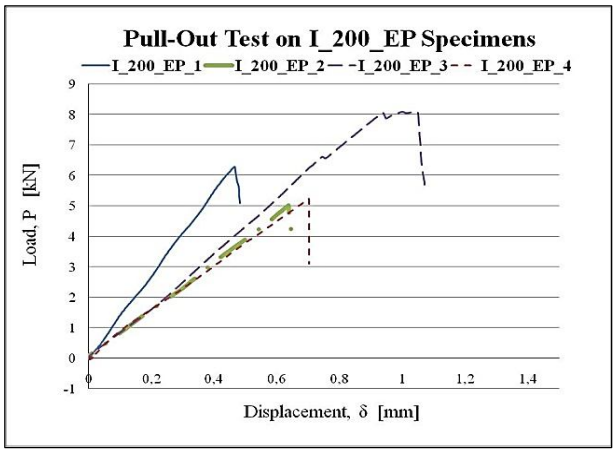

Figure 6. Load (P) versus displacement (δ) curve for *I_200_EP* group of specimens.

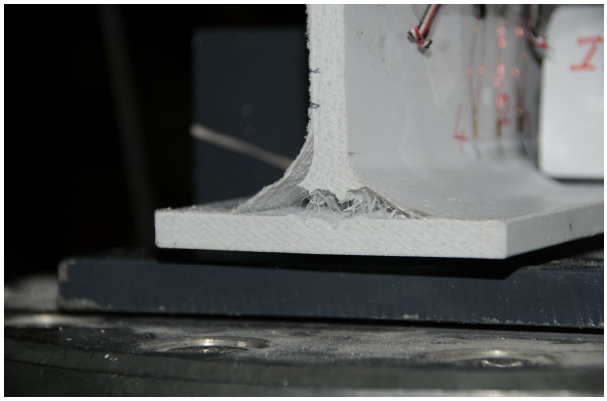

Figure 7a. Failure mode of I_*200_MP_1* specimen**.**

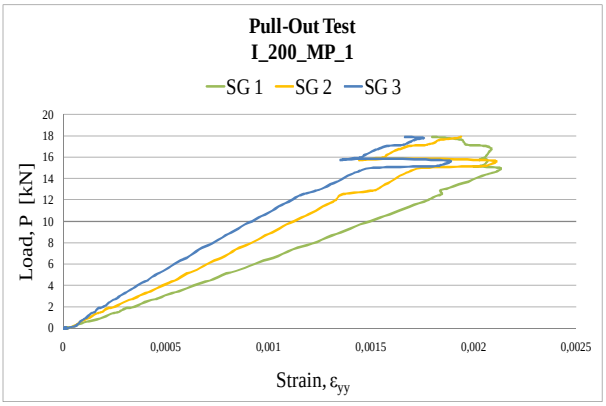

Figure 7b. Load (P) versus experimental strain (ε_{yy}) of *I_200_MP_1* specimen.

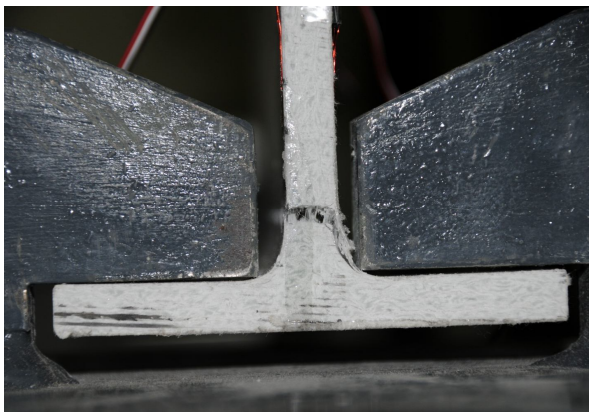

Figure 8a. Failure mode of I_*200_EP_1* specimen**.**

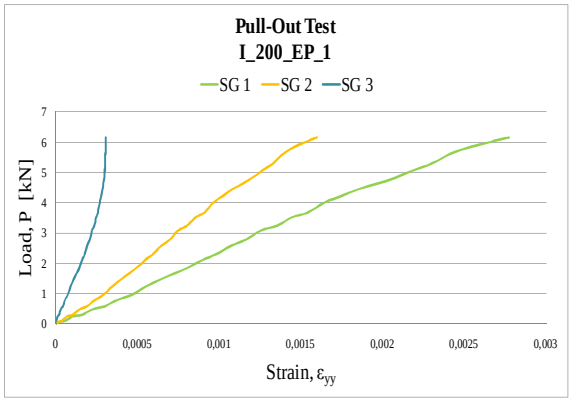

Figure 8b. Load (P) versus experimental strain (ε_{yy}) of I_*200_EP_1* specimen.

Figure 9a. Failure mode of I_*200_EP_2* specimen**.**

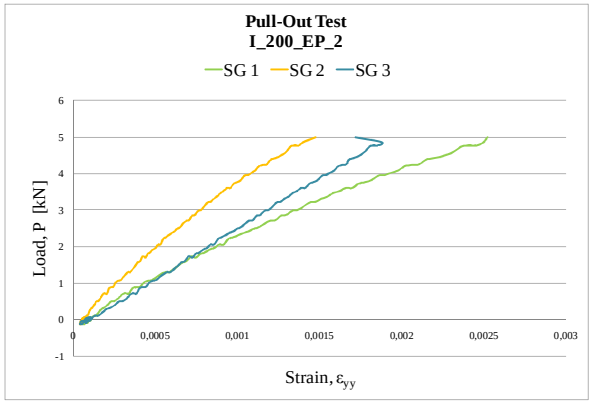

Figure 9b. Load (P) versus experimental strain (ε_{yy}) of *I_200_EP_2* specimen.

For specimens *I_200_EP_2* and *I_200_MP_1*, the simulation strains results along the y-axis (ε_{yy}), obtained at the load levels of 5.0063 kN (failure load) and 12.3199 kN, respectively, were compared with the corresponding experimental data measured at the points SG1, SG2 and SG3 where the strain gages were placed (Figs. 11a and 11b). In both cases, a reasonably good agreement between the simulation and the real data can be observed.

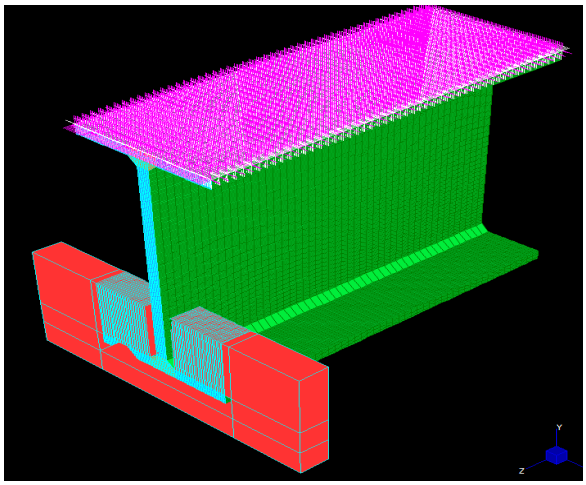

Figure 10a. Finite-element model of *I_200_EP_1* (*I_200_EP_2*) specimens.

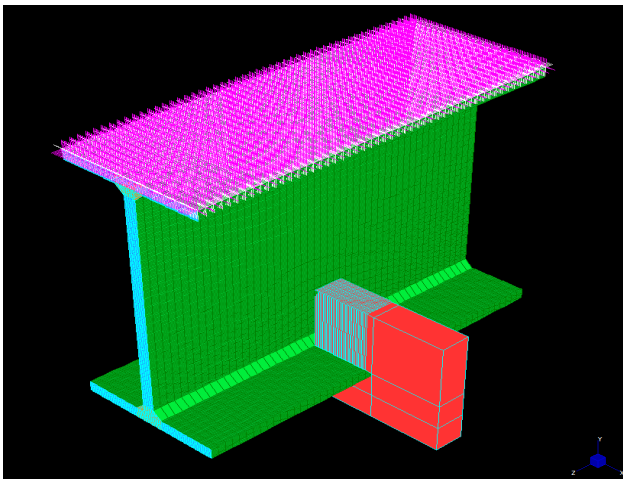

Figure 10b. Finite-element model of *I_200_MP_1* specimens.

Finally, the stress-concentrations (σ_{yy}) at the web-flange junction of the two specimens are presented in Figs. 12a and 12b. From these figures, one can notice the different stress distributions produced from the numerical analysis, as well as the different failure modes observed during this preliminary experimental study. The two modes of failure were in the form of (*i*) a complete and sudden separation of the flange from the web (see Figs. 7a and Fig. 8a), or (*ii*) a progressive failure in the form of a delamination crack adjacent to the triangular shaped core of roving (refer to Fig. 9a).

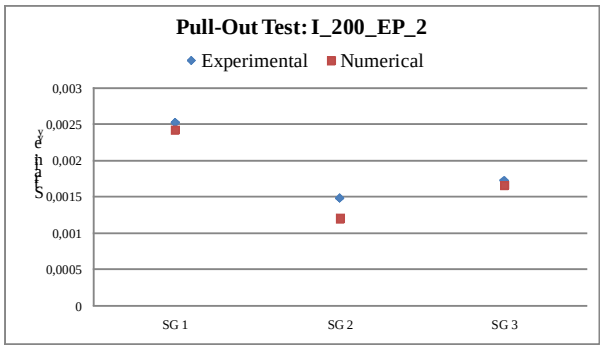

Figure 11a. Comparisons of the experimental and numerical results of ε_{yy} in the pull-out test of I_*200_EP_2* specimen ($P=P_{failure}$=5.0063kN).

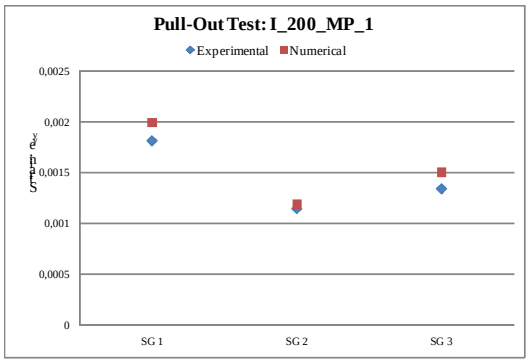

Figure 11b. Comparisons of the experimental and numerical results of ε_{yy} in the pull-out test of I_*200_MP_1* specimen (P=12.3199kN).

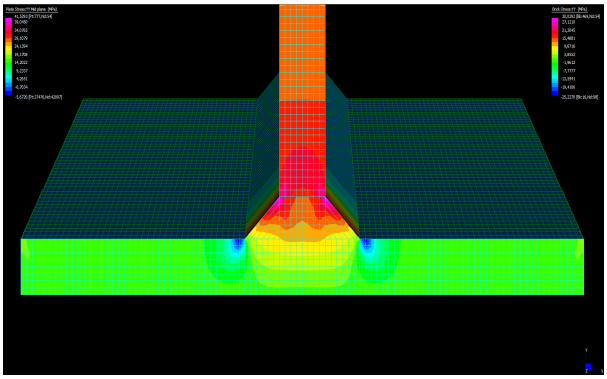

Figure 12a. Stress concentration (σ_{yy}) at the web-flange junction of the end point of *I_200_EP_2* specimen (*P=5.0063kN*).

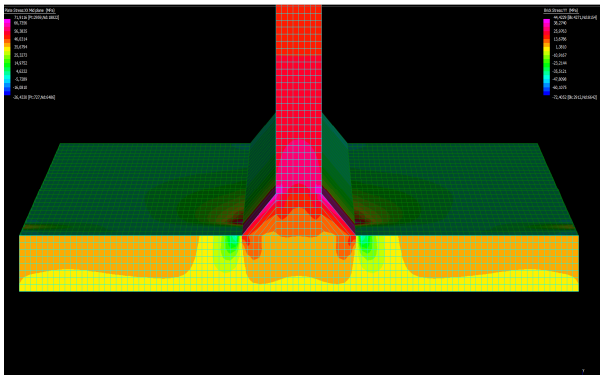

Figure 12b. Stress concentration (σ_{yy}) at the web-flange junction of the mid point of *I_200_MP_1* specimen (*P=12.3199kN*).

5 Conclusions

Preliminary experimental and numerical results of a pilot study, aimed at evaluating the web/flange axial strength and stiffness of fifteen PFRP are presented. 3-D finite element models were developed to predict the behavior of these specimens. Results from the numerical models were compared to those obtained from the experimental program and found to be satisfactory.

The results gathered from this preliminary pilot research study provide important information on one major structural deficiency and limitations related to the inherent weakness of the web/flange junctions of the majority of commercially produced, off-the-shelf unidirectional pultruded composites.

The results of this research will provide structural engineers with essential design data to assist to secure optimum design as well as to achieve maximum benefits of PFRP materials.

Acknowledgments

The authors gratefully acknowledge the financial support of Italian MIUR (*PRIN 20089RJKYN_003*), the Italian Department of Civil Protection and the Laboratories University Network of Seismic Engineering (*DPC_ReLUIS Project 2010-2013*). Special thanks to *Saimex S.r.l. (Seregno, Milan, Italy)* for donating of the PFRP materials evaluated in this study.

References

[1] Mosallam A.S., Elsadek A.A., Pul S. *Semi-rigid behavior of web-flange junctions of open-web pultruded composites* in Proceeding *of the International Conference on FRP Composites*, San Francisco, California (2009).

[2] Mosallam A.S., Bank L.C. Short-term behavior of pultruded fiber reinforced plastic frame. *Journal of Structural Engineering (ASCE)*, **118(7)**, pp. 1037–1954 (1992).

[3] Mosallam A.S., Abdelhamid M.K. *Dynamic behavior of PFRP structural Sections*, in Proc. of ASME (Energy Sources Tech. Conf. and Expo, Composite Material Tech.), **53**, pp. 37–44 (1993).

[4] Davalos J.F., Salim H.A., Qiao P., Lopez-Andio R. Analysis and design of pultruded FRP shapes under bending. *Composites Part B: Engineering*, **27B(3,4)**, pp. 295–305 (1996).

[5] Mosallam A.S., Abdelhamid M.K., Conway J.H. Performance of pultruded FRP connection under static and dynamic loads. *Journal of Reinforced Plastic and Composites*, **13**, pp. 1052–1067 (1996).

[6] Liu X., Mosallam A.S., Kreiner J. *A numerical investigation on static behavior of pultruded composite (PFRP) portal frame structures* in *Proceeding of the 43rd International SAMPE Symposium and Exhibition*, Anaheim, California (1998).

[7] Mosallam A.S. *Durability of pultruded fiber reinforced polymer (PFRP) composites in mining environments* in Durability of fiber reinforced polymer (FRP) composites for construction, Edited by B. Benmokrane and H. Rahman, pp. 649-659 (1998).

[8] Turvey G.J., Zhang Y. Characterisation of the rotational stiffness and strength of web-flange junctions of pultruded GRP WF-sections via web bending tests. *Composites Part A: applied science and manufacturing*, **37**, pp. 152–164 (2006).

[9] Turvey G.J, Zhang Y. Shear failure strength of web-flange junctions in pultruded GRP WF profiles. *Construction and Building Materials*, **20**, pp. 81–89 (2006).

[10] Ascione L., Feo L. *Mechanical behavior of composites for construction* in "Wiley Encyclopedia of Composites", Second Edition, Edited by L. Nicolais and A. Borzacchiello. John Wiley & Sons (2012).

[11] Mosallam A.S. *Design for FRP Composite Connections* in "ASCE Manuals and Reports on Engineering Practice #102", American Society of Civil Engineers (ASCE), Virginia, (2011). *In press*.